

# A Comparison in Monkeys of $^{99m}\text{Tc}$ Labeled to a Peptide by 4 Methods

Mary Rusckowski, Tong Qu, Suresh Gupta, Arthur Ley, and Donald J. Hnatowich

Division of Nuclear Medicine, Department of Radiology, University of Massachusetts Medical School, Worcester; and Dyax Corporation, Cambridge, Massachusetts

Although a number of different strategies for labeling peptides with  $^{99m}\text{Tc}$  have been developed, only a few studies have compared the in vivo properties of  $^{99m}\text{Tc}$  when attached to different chelators. Furthermore, these comparisons are usually in mice, whereas results obtained in nonhuman primates may be expected to be more relevant to the clinical situation. **Methods:** We evaluated the influence of 4 common chelators on the biodistribution in monkeys of  $^{99m}\text{Tc}$ -labeled HNE-2, a 6.7-kDa peptide being investigated as an inflammation/infection imaging agent. The peptide was conjugated with the *N*-hydroxysuccinimide ester of mercaptoacetyltriglycine (MAG3), mercaptoacetyltriserine (MAS3), hydrazinonicotinamide (HYNIC), and the cyclic anhydride of diethylenetriaminepentaacetic acid (DTPA). After radiolabeling, each peptide was administered intravenously to rhesus monkeys with a *Staphylococcus aureus*-induced focal inflammation/infection. **Results:** Quantification of radioactivity accumulation by regions of interest over 3 h after administration in monkeys showed important differences among labeling methods: For example, at 3 h, kidney accumulation varied in percentage injected dose per organ (%ID per organ) from 31 %ID per organ (HYNIC) to 18 %ID per organ (MAG3), whereas liver varied from 7.8 %ID per organ (MAG3) to 2.8 %ID per organ (MAS3). Radioactivity accumulation in the lesion was independent of labeling method. These organ accumulations were compared with that obtained earlier in mice by sacrifice and dissection also at 3 h and at the same administered dosage. In the rodent, kidney levels varied from 45 %ID per organ (HYNIC) to 12 %ID per organ (MAS3) and liver levels varied from 6.5 %ID per organ (DTPA) to 2.0 %ID per organ (MAS3). **Conclusion:** In agreement with previous work from this laboratory and elsewhere, the method of radiolabeling had an important effect on the biodistribution of  $^{99m}\text{Tc}$ . Furthermore, although biodistribution results in mice should be used with caution to predict biodistributions in primates, in major organs, these results in mice and monkeys were similar.

**Key Words:**  $^{99m}\text{Tc}$ -peptides; MAG3; mercaptoacetyltriserine; hydrazinonicotinamide; DTPA dianhydride

**J Nucl Med 2001; 42:1870–1877**

The use of small, labeled peptides as radiopharmaceuticals is an area that has seen a growing number of applications in recent years. Peptides have been labeled with a number of isotopes, although  $^{99m}\text{Tc}$  remains one of the most useful for single-photon diagnostic imaging.  $^{99m}\text{Tc}$ -Labeling strategies for peptides have been reviewed extensively (1–3), and this laboratory has investigated various  $^{99m}\text{Tc}$ -labeling strategies from a growing list of bifunctional chelators (4–6). As this laboratory and others have shown, the method selected for  $^{99m}\text{Tc}$  labeling can have a pronounced effect on the properties of the label in vitro and in vivo (7–11). Previously, we reported on 2 similar human neutrophil elastase inhibitor peptides, EPI-HNE-2 (HNE-2) and EPI-HNE-4 (HNE-4) (7,12), labeled with  $^{99m}\text{Tc}$  using 3 bifunctional chelators: the *N*-hydroxysuccinimide ester of *S*-acetyl mercaptoacetyltriglycine (MAG3) (4), the cyclic anhydride of diethylenetriaminepentaacetic acid (DTPA) (13), and the *N*-hydroxysuccinimide ester of hydrazinonicotinamide (HYNIC) (14). On the basis of those results, we concluded that it may be important to compare chelators and labeling methods before selecting a  $^{99m}\text{Tc}$ -labeling method for any particular peptide.

In this investigation, we describe a biodistribution study using an existing nonhuman primate model for in vivo inflammation/infection imaging (15). The peptide HNE-2 was radiolabeled with  $^{99m}\text{Tc}$  using 1 of 4 bifunctional chelators: *N*-hydroxysuccinimidyl (NHS)-*S*-acetyl-MAG3, NHS-*S*-acetylmercaptoacetyltriserine (MAS3) (5), NHS-HYNIC (with tricine as coligand), and the cyclic anhydride of DTPA. Previously we used these same 4 methods to prepare  $^{99m}\text{Tc}$ -radiolabeled HNE-2 for studies in healthy mice. The results obtained in both species are now compared.

## MATERIALS AND METHODS

Standard chemicals were obtained from various suppliers and used without purification.  $^{99m}\text{Tc}$ -Pertechnetate was obtained from a  $^{99}\text{Mo}$ - $^{99m}\text{Tc}$  radionuclide generator (Dupont Pharma Radiopharmaceuticals, Billerica, MA). The peptide HNE-2 was a gift from Dyax Corp. (Cambridge, MA) and was selected from a phage library as a potent (inhibition constant, 2 pmol/L) neutrophil elastase-specific inhibitor (12). The native HNE-2 has a molecular weight of 6.7 kDa and 2 lysines plus the terminal amine available for conjugation. The synthesis of NHS-MAG3 (4) and NHS-

Received Apr. 6, 2001; revision accepted Aug. 20, 2001.

For correspondence or reprints contact: Mary Rusckowski, PhD, Division of Nuclear Medicine, Department of Radiology, University of Massachusetts Medical School, 55 Lake Ave. N., Worcester, MA 01655-0243.

HYNIC (14) were as described. The NHS-MAS3 synthesis and its use as an alternative to NHS-MAG3 also has been described (5).

### Conjugation and Radiolabeling

**NHS-MAG3 and NHS-MAS3.** The conjugation and radiolabeling with  $^{99m}\text{Tc}$  of MAG3-conjugated peptides has been described (16). Briefly, for conjugation with NHS-MAG3 the HNE-2 peptide was first prepared at a concentration of 5 mg/mL in 0.1 mol/L *N*-(2-hydroxyethyl)piperazine-*N'*-(2-ethanesulfonic acid (HEPES) buffer, pH 8.0, to which a fresh 10 mg/mL solution of NHS-MAG3 in dry dimethylformamide (DMF) was added dropwise with agitation. The final MAG3-to-peptide molar ratio was 3:1, and the volume of DMF added was always <10% of the total volume. The reaction mixture was then incubated at room temperature for 30–60 min before purification on a  $0.7 \times 20$  cm P4 size-exclusion open column (BioRad, Hercules, CA) with 0.25 mol/L ammonium acetate, pH 5.2, eluant. Fractions were collected and quantitated by ultraviolet (UV) absorbance at 280 nm (U-2000; Hitachi Instruments, Inc., Danbury, CT) using an extinction coefficient of 0.89 for HNE-2.

For radiolabeling, the conjugated peptide was diluted to approximately 0.4–0.5 mg/mL with 0.25 mol/L ammonium acetate, pH 5.2. To 0.25 mL of the coupled peptide solution was added an aliquot of sodium tartrate prepared to 50 mg/mL in 0.5 mol/L sodium bicarbonate, 0.25 mol/L ammonium acetate, and 0.175 mol/L ammonium hydroxide buffer, pH 9.2, for a final tartrate concentration of 7  $\mu\text{g}/\text{mL}$  (for labeling at pH 7.6). After adding approximately 111 MBq  $^{99m}\text{Tc}$ -pertechnetate generator eluant, 7  $\mu\text{L}$  of a fresh solution of  $\text{SnCl}_2 \cdot 2\text{H}_2\text{O}$  (1 mg/mL in 10 mmol/L HCl) were added. The solution was then incubated at room temperature for 30–60 min before purification over the P4 column with 50 mmol/L phosphate-buffered saline (PBS), pH 7.2, as eluant. Those fractions with the highest radioactivity were pooled and the protein concentration was determined by UV absorbance at 280 nm. The sample was analyzed for radiochemical purity using a C18 Sep-Pak mini cartridge (Waters, Milford, MA) as follows. After preconditioning with 10 mL ethanol followed by 10 mL water, an aliquot of labeled peptide sample was applied and the column was washed with 5 mL 1 mmol/L HCl to elute  $^{99m}\text{Tc}$ -tartrate and  $^{99m}\text{Tc}$ -pertechnetate. The labeled peptide was then recovered with a 1:1 solution of ethanol and saline, and the radiochemical purity was calculated. Finally, for administration, the labeled peptide was sterilized by passage through a 0.22- $\mu\text{m}$  filter (Gelman Sciences, Ann Arbor, MI). The conjugation and radiolabeling of the peptide with NHS-MAS3 was identical to that described above for MAG3.

**Cyclic Anhydride of DTPA.** The DTPA-conjugated peptide was prepared as follows. To a 10 mg/mL solution of the peptide in water was added an equal volume of 0.2 mol/L HEPES buffer, pH 8.0. A suspension of the DTPA cyclic anhydride (Sigma Chemical Co., St. Louis, MO) in DMF (10 mg/mL) was then added dropwise with agitation to a final DTPA-to-peptide molar ratio of 3:1. After 30 min at room temperature, the coupled peptide was purified on the P4 column as described above. For radiolabeling with  $^{99m}\text{Tc}$ , 0.05 mL DTPA-peptide solution ( $\sim 2.0$  mg/mL in 0.25 mol/L ammonium acetate buffer, pH 5.2) was added to 18  $\mu\text{L}$  of a buffer consisting of 0.5 mol/L sodium bicarbonate, 0.25 mol/L ammonium acetate, and 0.175 mol/L ammonium hydroxide, pH 9.2. To this was added approximately 148 MBq  $^{99m}\text{Tc}$ -pertechnetate (20–40  $\mu\text{L}$ ) followed immediately by addition of 6–12  $\mu\text{L}$  of a fresh solution of  $\text{SnCl}_2 \cdot 2\text{H}_2\text{O}$  (1 mg/mL in 10 mmol/L HCl). After 30 min at room temperature, the preparation was purified over the

P4 column with 50 mmol/L PBS (pH 7.2) eluant. Analysis and sterilization for administration were similar to those described above for MAG3.

**NHS-HYNIC.** The peptide was conjugated with NHS-HYNIC using a 3:1 HYNIC-to-peptide molar ratio as described (7) followed by purification on the P4 column as described above. Approximately 20  $\mu\text{L}$  of a 0.1 mg/mL tricine solution in water was added to approximately 0.1 mg of the HYNIC-peptide in 0.1 mL of 0.25 mol/L ammonium acetate, pH 5.2, to which was added approximately 111 MBq  $^{99m}\text{Tc}$ -pertechnetate generator eluant, followed by addition of 6  $\mu\text{L}$  fresh  $\text{SnCl}_2 \cdot 2\text{H}_2\text{O}$  (1 mg/mL in 10 mmol/L HCl) solution. After incubation at room temperature for 30–60 min, the labeled peptide was purified over the P4 column with 50 mmol/L PBS (pH 7.2). Analysis and preparation for administration were similar to those described above for MAG3.

### Serum Stability

Size-exclusion high-performance liquid chromatography (HPLC) analysis was used to estimate the stability of  $^{99m}\text{Tc}$  on each peptide preparation toward incubation at 37°C in fresh human serum. All radiolabeled peptides were analyzed by size-exclusion HPLC using a  $1 \times 30$  cm Superdex-peptide column (Pharmacia, Piscataway, NJ), with 0.1 mol/L sodium phosphate, pH 7.0, as eluant and with in-line radioactivity and UV detection. The labeled peptides were added to 37°C serum at a concentration of approximately 1–5  $\mu\text{g}/\text{mL}$ , and samples were removed for analysis at various times from 5 min to 24 h. Recovery of radioactivity was routinely determined. A shift of the radioactivity profile to higher molecular weight could signify serum protein binding, whereas the presence of lower-molecular-weight peaks could signify a breakdown to labeled catabolites or dissociation of the label.

### Mouse Biodistribution

All animal studies were performed with the approval of the Institutional Animal Care and Use Committee. In groups of 5, normal CD-1 male mice ( $\sim 28$  g; Charles River, Wilmington, MA) were injected through a tail vein with 0.1 mL 50 mmol/L PBS containing 1–2  $\mu\text{g}$  (370–740 kBq) labeled peptide. At 3 h, animals were anesthetized with metofane (Schering-Plough, Omaha, NE) and killed by cervical dislocation. Whole blood was collected and tissues of interest were removed for counting in a NaI(Tl) well counter along with a standard of the injectate.

### Inflammation Model

Five rhesus macaque monkeys (Michigan Biologic Products Institute, Lansing, MI), weighing 10–15 kg each, were used. The inflammation/infection model has been described (15). In brief, the inflammation was induced by the subcutaneous administration of a uniform suspension of *Staphylococcus aureus* cell products (Sigma; 6 mg/0.4 mL sterile saline), to which was added 50 mg arachidonic acid (Sigma). The animals were injected intramuscularly with 20 mg/kg of ketamine (Fort Dodge Laboratories, Inc., Fort Dodge, IA). The target area (lower back) was shaved and swabbed with alcohol, and the mixture of *S. aureus* and arachidonic acid was administered subcutaneously. The lesion typically resolved within a few days and the animals showed no signs of systemic infection. The radiolabeled peptide was administered 1 d after infection.

### Imaging Protocol

Scintigrams were acquired on a portable large field-of-view scintillation camera (Elsint, Hackensack, NJ) equipped with a

parallel-hole, low-energy collimator and an Elscint APEX F1 computer. Animals were positioned posteriorly on the collimator, and radioactivity was counted for 30–480 s using a  $512 \times 512$  matrix with a 20% energy window set at 140 keV. Before imaging, each animal was anesthetized with ketamine and intubated with an uncuffed tracheal tube (Mallinckrodt Medical Inc., St. Louis, MO). Animals received 2% isoflurane (Abbott Laboratories, North Chicago, IL) in oxygen to maintain anesthesia.

A total of 10 imaging studies were performed, 3 each with MAG3 and MAS3 and 2 each with DTPA and HYNIC. Assignment of monkeys and labeling method were random. The dosage of peptide ranged between 42 and 67  $\mu\text{g}$  labeled with 26–39 MBq. The injectate was administered as a bolus through an in-line catheter in a right arm vein and was followed by a saline flush. Images were acquired immediately and for the next 4 h. Approximately 10 min after injection of the labeled peptide, and throughout the imaging period, lactated Ringer's solution (Baxter Health Care, Deerfield, IL) was infused through the catheter at a rate of approximately 24 mL/h to maintain electrolyte balance.

For analysis of the whole-body images, regions of interest were placed about the left and right kidneys, the liver, the lesion (lower back), and a contralateral area of the lower back for background subtraction. Counts were recorded without absorption correction. An estimate of the radioactivity in becquerels within each region was obtained by applying the counts to a calibration curve of counts per minute versus becquerels obtained using standard solutions of  $^{99\text{m}}\text{Tc}$ . Results were then normalized to the radioactivity administered.

### Plasma Collection

Blood samples of approximately 0.2 mL were obtained by a direct needle stick, transferred to a Vacutainer tube (Becton-Dickinson, Franklin Lakes, NJ) coated with ethylenediaminetetraacid, and immediately placed on ice for plasma analysis. After separation, samples of plasma were counted for radioactivity against a standard of the injectate so that the results could be presented as percentage injected dose (%ID) per milliliter. Samples were also analyzed by size-exclusion HPLC as described above. Plasma not analyzed immediately was stored at 4°C.

## RESULTS

### Radiolabeling

Radiolabeling efficiencies ranged between 44% and 85% and were independent of the method and the chelator used. After P4 column purification, the average radiochemical purity for all preparations by Sep-Pak analysis was  $88.5\% \pm 4.6\%$  (mean  $\pm$  SD). No attempt was made to maximize specific activity.

### In Vitro Serum Incubation

Size-exclusion HPLC radiochromatograms of in vitro 37°C serum incubations for HNE-2 radiolabeled through MAG3 and DTPA at pH 7.6 and HYNIC have been presented previously (7). The radiochromatograms obtained in this investigation for HNE-2 radiolabeled through MAS3 were similar. After only 5 min of incubation in serum, radioactivity associated with higher-molecular-weight peaks was evident for each preparation, probably as a result of protein binding. In each case, the radioactivity associated with

higher-molecular-weight peaks increased with additional incubation time. Distinct minor species of low molecular weight became apparent in the 1-h chromatograms in all cases. Species eluting in these later fractions have been identified previously as radiolabeled cysteine resulting from the transchelation of the label from peptide to endogenous cysteine (17,18), as may be the case here.

### Biodistribution

Plasma clearance curves in monkeys for  $^{99\text{m}}\text{Tc}$  radiolabeled to HNE-2 are presented in Figure 1. These data are averages obtained from 2 or 3 studies with each chelator. Plasma clearance rates were rapid and were similar for 3 chelators: MAG3, MAS3, and HYNIC. Circulating levels of radioactivity decreased to  $<0.1$  %ID by 30–40 min after administration, and circulating levels at 3–4 h were 0.02–0.04 %ID. However, when HNE-2 was labeled using DTPA, plasma clearance was approximately 2-fold slower.

Figure 2 shows HPLC radiochromatograms of  $^{99\text{m}}\text{Tc}$  in plasma collected from monkeys at 5–60 min. For comparison, a radiochromatogram of each labeled HNE-2 in saline is also presented (Fig. 2A). As early as 5 min (Fig. 2B), multiple high-molecular-weight peaks are clearly evident in the MAG3, MAS3, and HYNIC samples. By 30 min, for all 4 chelators (Fig. 2C), about half of the radioactivity in plasma eluted with an earlier retention time than did the labeled peptide in saline, most probably because of serum protein binding.

Average radioactivity levels in liver from 0 to 4 h are presented in Figure 3. Important differences in liver activity are evident among the various labeling methods, with the highest levels obtained using MAG3, whereas MAS3 provided the lowest levels by a factor of approximately 3. Average radioactivity levels in kidneys are shown in Figure 4. Kidney levels for HYNIC and MAS3 were indistinguishable and were nearly 2-fold higher than those for DTPA and MAG3.

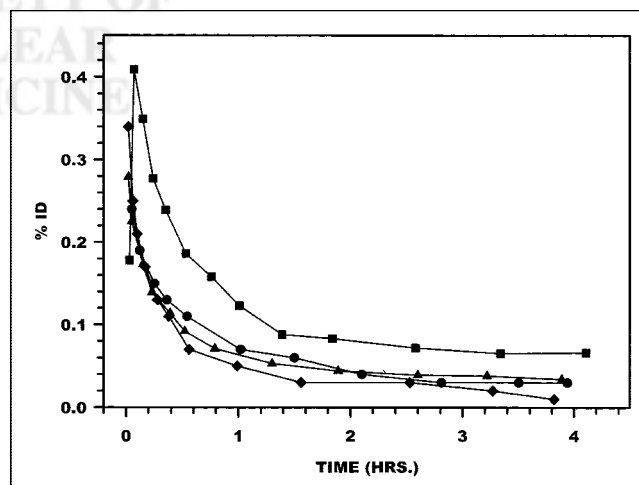
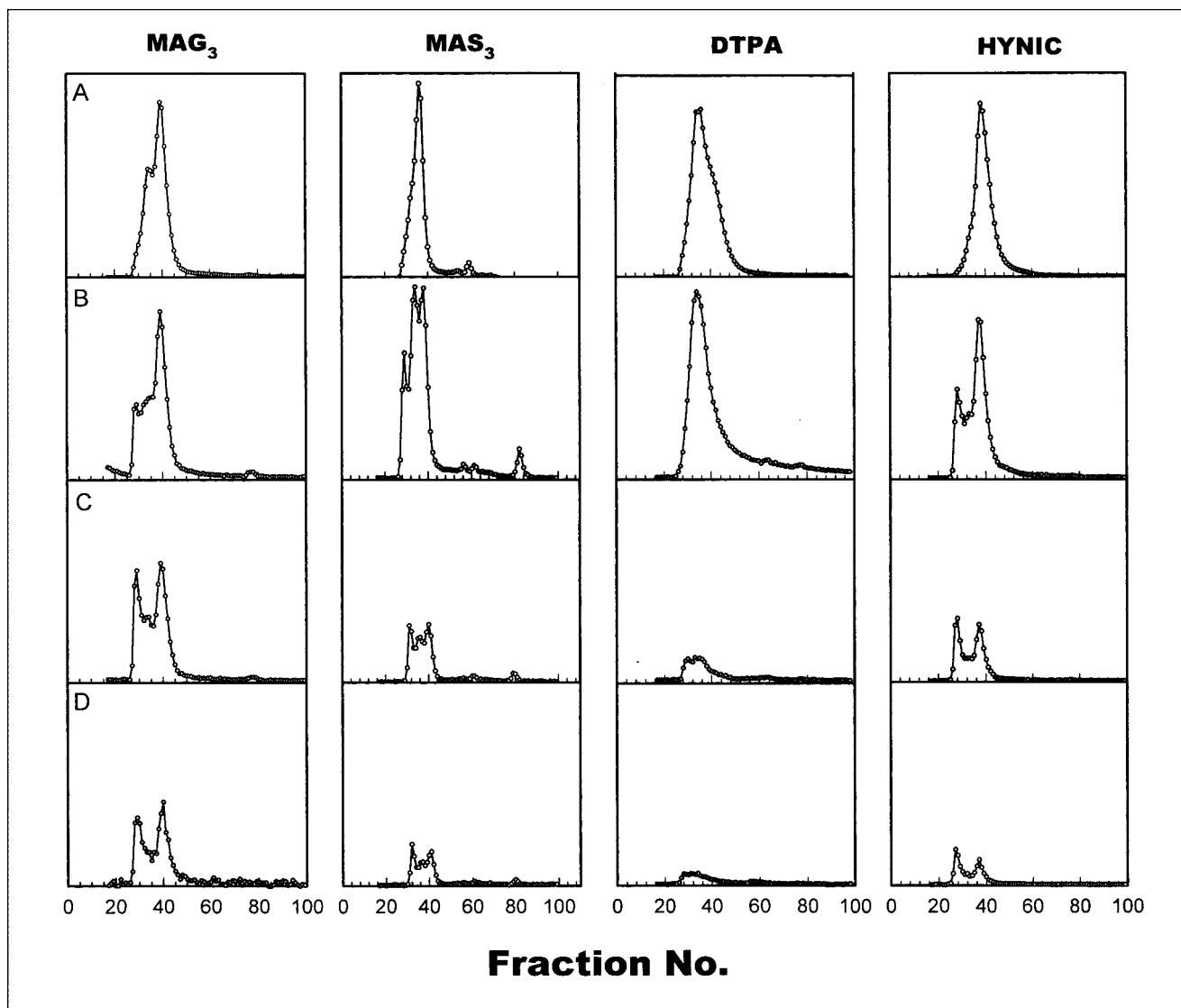


FIGURE 1. Clearance from plasma of  $^{99\text{m}}\text{Tc}$  labeled to HNE-2 using MAG3 (●), MAS3 (◆), DTPA (■), and HYNIC (▲).



**FIGURE 2.** Size-exclusion HPLC radiochromatograms of <sup>99m</sup>Tc labeled to HNE-2 using 4 chelators in saline (A) and in plasma collected from monkeys at 5 min (B), 13–30 min (C), and 60 min (D).

Radioactivity accumulations in the lesion showed no differences among the labeling methods. However, as shown in Figure 5, when presented as lesion-to-plasma ratios (i.e., %ID in the lesion compared with plasma radioactivity per milliliter), DTPA showed the lowest ratio at all time points.

#### Comparative Biodistributions

Table 1 compares biodistribution in monkeys and mice of <sup>99m</sup>Tc in %ID per total organ at 3 h after IV administration of radiolabeled HNE-2. The dosage was 3–67 μg/kg in mice, and for monkeys the dosage was 3–7 μg/kg. Results in Table 1 for radiolabeled MAG<sub>3</sub>, HYNIC, and DTPA in mice have been reported previously (7). Data for the monkey are based on in vivo imaging data for which counts were obtained from within regions of interest placed about the liver, heart, kidneys, and spleen. For the mouse, entire organs were removed for counting in a well counter.

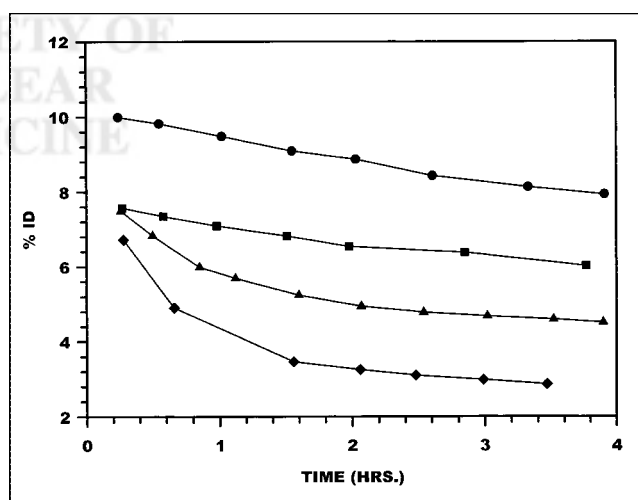


**FIGURE 3.** Radioactivity clearance in liver (%ID) over 4 h for HNE-2 labeled using MAG<sub>3</sub> (●), MAS<sub>3</sub> (◆), DTPA (■), and HYNIC (▲). Data points represent averages (*n* = 2 or 3) for each chelator.

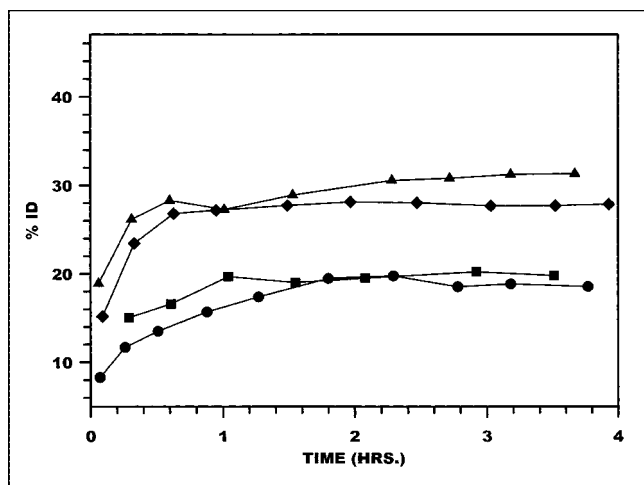


**FIGURE 4.** Radioactivity clearance in kidneys (%ID) over 4 h for HNE-2 labeled using MAG3 (●), MAS3 (◆), DTPA (■), and HYNIC (▲). Data points represent averages ( $n = 2$  or 3) for each chelator.

Organ radioactivity levels shown in Table 1 are generally higher in monkeys compared with mice. Contributions from overlying and underlying tissues can be expected to result in an overestimate of in vivo organ radioactivity levels. An overestimate would be expected to be most serious for those organs with lower levels of accumulations, such as heart and spleen. These effects are evident in the data shown in Table 1.

Figure 6 illustrates the correlation between the mouse and monkey data of Table 1. A logarithm-logarithm scale is used to accommodate the wide dynamic range of these data. The solid line in Figure 6 depicts the behavior expected if the relationship between the 2 datasets was exact. Whenever the mouse values are relatively high ( $>1\%$ ), a good correlation is apparent despite the differences in dosage. Whenever the mouse values are less than approximately 1% (e.g., heart and spleen), the correlation between the mouse and monkey datasets is less exact, presumably because of contributions from background radioactivity levels to the primate measurements. Clearly, the exact size and position of the area of interest will influence the magnitude of the background contribution.

A composite of scintigraphic images is shown in Figure 7. The images are from 3 h after administration, with 1 example shown for each of the 4  $^{99m}\text{Tc}$ -chelate preparations. The images are shown to emphasize the difference in clearance and organ accumulation of the 4 chelate complexes. For example, liver is highest with MAG3 and lowest with MAS3.

## DISCUSSION

It has become evident that for peptides, possibly because of their relatively small size, the choice of chelating agent can influence the in vitro properties and the biodistribution of  $^{99m}\text{Tc}$  (7-11). Previously, this laboratory showed in the

same monkey model that  $^{99m}\text{Tc}$ -MAG3-HNE-2 localized rapidly and specifically in sites of infection/inflammation (15). The principal aim of this study was to use the nonhuman primate infection model to compare the properties of  $^{99m}\text{Tc}$  attached to HNE-2 by 4 different chelating agents. A second aim was to compare the biodistribution of  $^{99m}\text{Tc}$  in major organs between monkeys and healthy mice administered radiolabeled peptides differing only in the nature of the chelating agent.

In a previous investigation (7), size-exclusion HPLC analysis of radiolabeled peptides incubated in serum in vitro showed evidence for serum protein binding within 5 min of incubation. Serum protein binding is also the most likely explanation for the shift in radioactivity to earlier retention times seen in the radiochromatograms of plasma samples obtained from monkeys in this investigation (Fig. 2). Distinct low-molecular-weight species were not prominent in any of the radiochromatograms, although DTPA showed a small broad peak at longer elution times. Therefore, the slower plasma clearance of DTPA relative to that of the remaining chelators (Fig. 1) cannot be attributed either to association with serum proteins or to label dissociation, but probably reflects a chelator-specific influence on clearance.

Major chelator-related differences in the biodistributions were observed in liver and kidneys. HNE-2 labeled using HYNIC and MAS3 showed the lowest accumulations in liver (Figs. 3 and 7) and the highest accumulations in kidneys (Fig. 4). Relative levels of radioactivity in these 2 organs may indicate the relative contributions of renal and hepatobiliary routes of clearance. For small peptides, the relative overall hydrophobicity of the peptide can substantially influence the route of biologic clearance (2). In general, hepatobiliary clearance is the major route for more hydrophobic peptides, such as formyl-Met-Leu-Phe (11), whereas more hydrophilic peptides, such as free MAG3

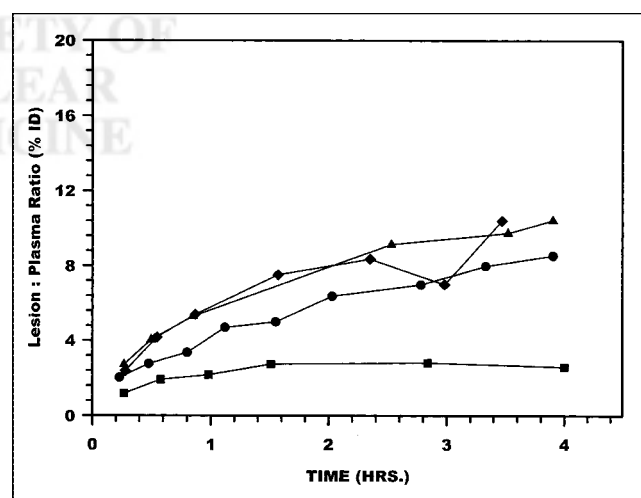


**FIGURE 5.** Radioactivity ratios between lesion (%ID) to plasma (%ID/mL) over 4 h for HNE-2 labeled using MAG3 (●), MAS3 (◆), DTPA (■), and HYNIC (▲).

**TABLE 1**  
Biodistribution of Labeled Peptides in Monkeys and in Mice

Organ	Monkey				Mouse*			
	MAG3	MAS3	HYNIC	DTPA	MAG3	MAS3	HYNIC	DTPA
Kidneys	18.4	27.5	31	19.4	15 ± 1.0	12 ± 2.12	45 ± 6.0	20 ± 1.0
Liver	7.8	2.8	4.6	5.5	2.3 ± 0.4	2 ± 0.23	3.2 ± 0.2	6.5 ± 0.3
Heart	1.3	0.6	1.7	1.2	0.03 ± 0.0	0.05 ± 0.01	0.11 ± 0.01	0.06 ± 0.01
Spleen	0.6	0.6	0.8	0.6	0.04 ± 0.0	0.05 ± 0.01	0.14 ± 0.02	0.2 ± 0.02

\*Values are expressed as mean ± SD.

Values are %ID per organ at 3 h after intravenous administration for each labeled preparation in both species. For monkey studies,  $n = 2$ , except for MAG3 and MAS3 ( $n = 3$ ). For mouse studies,  $n = 5$ .

(19), are cleared through renal filtration and excretion. The peptide HNE-2 contains a very hydrophobic solvent-exposed stretch of 5 amino acids (Ile-Ala-Phe-Phe-Pro) that confers the high affinity and specificity to human neutrophil elastase (12). It seems likely that the presence of this hydrophobic patch on the surface of the HNE-2 molecule

influences the distribution of the radiolabeled compound between routes of clearance in vivo. The presence of 1 or more chelating groups of differing polarities coupled to HNE-2 may further modulate this distribution. In particular, the change in chelator from MAG3 to the more polar, but otherwise similar, MAS3 is accompanied by substantial

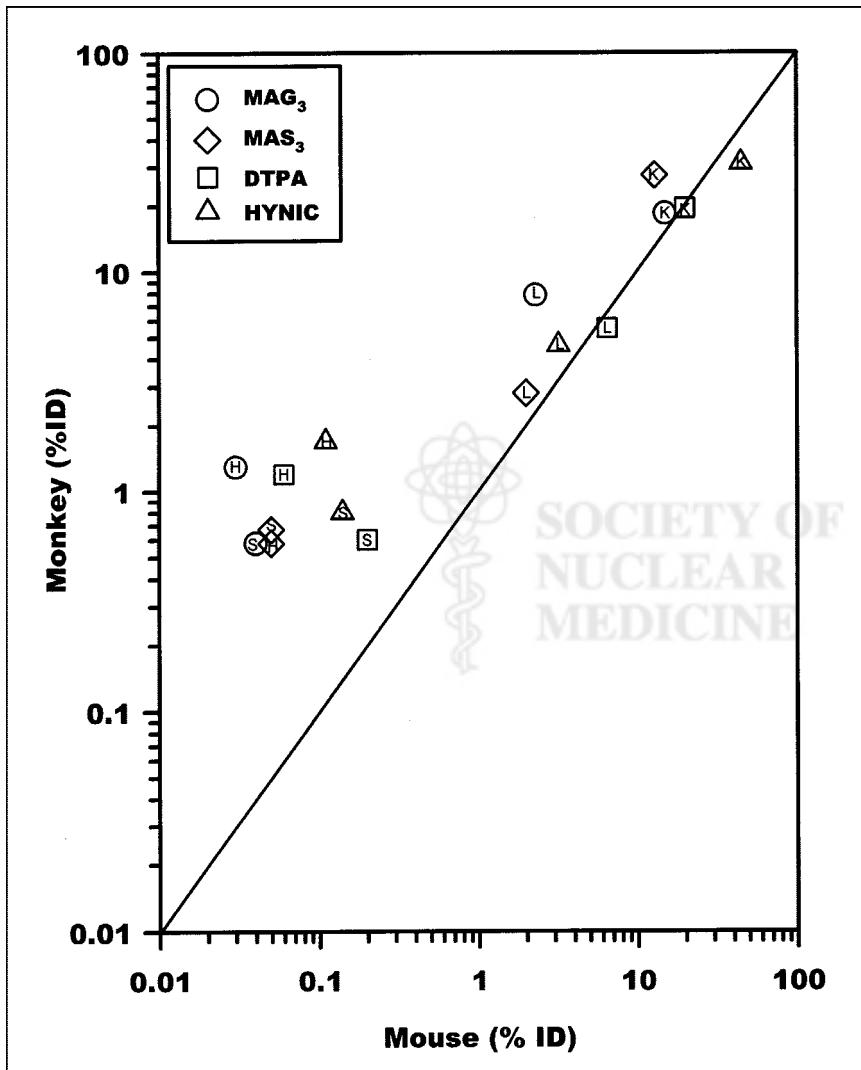


**FIGURE 6.** Logarithm-logarithm correlation plot of %ID per organ in monkey and mouse in kidney (K), liver (L), heart (H), and spleen (S). Data are taken from Table 1.

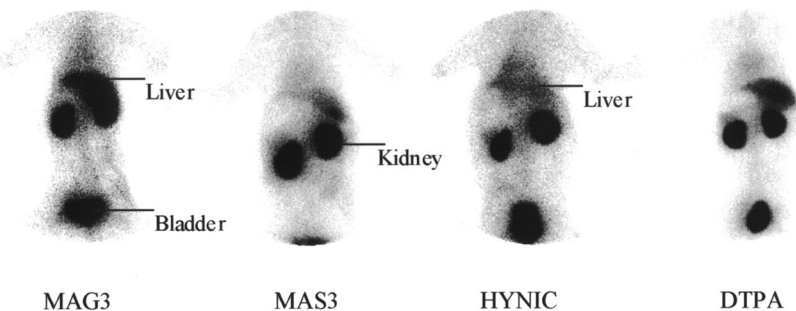


**FIGURE 7.** Composite of scintigraphic images in monkeys 3 h after administration, with 1 example shown for each of 4  $^{99m}\text{Tc}$ -chelate complexes.

decreases in liver and concomitant increases in kidney accumulations of radioactivity.

Accumulations of radioactivity in the lesion were similar for all 4 labeled HNE-2s. These *in vivo* results are therefore consistent with *in vitro* measurements showing that the methods of conjugating the peptide with bifunctional chelators do not influence the activity of the molecule toward human neutrophil elastase (15). However, when normalized to circulating plasma radioactivity, the DTPA-HNE-2 complex, relative to the other 3, showed a substantially lower level of target accumulation (Fig. 5). The DTPA-HNE-2 complex was also distinct among the 4 chelator-peptide complexes in showing a slower rate of plasma clearance and higher levels of circulating radioactivity at all times.

Overall, our results suggest that, among those considered, MAS3 is the preferred method for labeling HNE-2. This chelator is readily synthesized using inexpensive reagents and can be coupled with good efficiencies to HNE-2. The MAS3-HNE-2 complex retains the physicochemical stability properties of the unmodified molecule (A.C. Ley, unpublished data, 1999) along with accumulation in the intended target, human neutrophil elastase. The complex can be effectively and stably radiolabeled with  $^{99m}\text{Tc}$  without alteration of its properties. *In vivo*, the radiolabeled complex clears rapidly from circulation, accumulates rapidly and specifically at sites of infection/inflammation, and shows minimal levels of nonspecific organ accumulation.

The correlation between the mouse and monkey biodistribution datasets, shown in Figure 6, suggests that biodistribution data in mice are loosely predictive of the results in primates. As discussed above, the correlation between the datasets is less exact for low levels of organ radioactivity accumulation where, presumably, the methodology used to obtain the monkey data resulted in substantial overestimates of organ accumulations in some cases because of inclusion of background radioactivity. If so, extrapolation of the mouse data to primates may be more valid than that indicated by Figure 6 because the discrepancies may be the result of artifacts related to the noninvasive method used to estimate biodistributions in the monkey. Regardless, for most of the kidney and liver data listed in Table 1, the mouse and monkey accumulation levels agree to within a factor of 1.5. The 2 notable exceptions are the MAG3 liver data and the MAS3 kidney data, where the 2 sets differ by

factors of 2.5 and 2.2, respectively. However, the mouse data accurately predicted the large 3- to 10-fold differences in specific organ accumulation between the liver and kidney data in monkeys. Thus, such large differences in accumulation of radioactivity in specific organs for specific radiolabeled chelator-peptide complexes in mice may be predictive of similar large differences in the pharmacokinetics and biodistribution of the complexes in humans.

## CONCLUSION

In this investigation 1 peptide was radiolabeled with  $^{99m}\text{Tc}$  using 4 different chelators and tested in a nonhuman primate infection/inflammation model. Because we and others have previously observed an influence of labeling methods on the biodistribution of  $^{99m}\text{Tc}$  in mice when attached to small molecules such as HNE-2, an influence of labeling method on biodistribution was expected and was again observed, now in monkeys. Accordingly, we again conclude that the method selected for labeling peptides is likely to influence the properties of the radiolabel. More surprisingly perhaps, we observed a weak but possibly useful correlation between radioactivity accumulations in several organs, especially liver and kidneys, between monkeys and mice. We conclude that biodistribution studies of different labeling methods in mice may provide an indication of the influence of these labeling methods on the biodistribution in monkeys, at least in major organs.

## ACKNOWLEDGMENTS

The authors are grateful to Dyax Corporation for providing the HNE-2 and for providing partial financial support for this research.

## REFERENCES

- Liu S, Edwards DS, Barrett JA.  $^{99m}\text{Tc}$  labeling of highly potent small peptides. *Bioconj Chem*. 1997;8:621-636.
- Lister-James J, Moyer BR, Dean RT. Small peptides radiolabeled with  $^{99m}\text{Tc}$ . *Q J Nucl Med*. 1996;40:221-233.
- Liu S, Edwards DS.  $^{99m}\text{Tc}$ -labeled small peptides as diagnostic radiopharmaceuticals. *Chem Rev*. 1999;99:2235-2268.
- Winnard P Jr, Chang F, Rusckowski M, Mardirossian G, Hnatowich DJ. Preparation and use of NHS-MAG3 for technetium-99m labeling of DNA. *Nucl Med Biol*. 1997;24:425-432.
- Chang F, Qu T, Rusckowski M, Hnatowich DJ. NHS-MAS3: a bifunctional chelator alternative to NHS-MAG3. *Appl Radiat Isot*. 1999;50:723-732.
- Zhu Z, Wang Y, Rusckowski M, Hnatowich DJ. A novel and simplified route to

- the synthesis of N3S chelators for  $^{99m}\text{Tc}$  labeling. *Nucl Med Biol.* 2001;28:703–708.
7. Qu T, Wang Y, Zhu Z, Rusckowski M, Hnatowich DJ. Different chelators and different peptides together influence the in vitro and mouse in vivo properties of  $^{99m}\text{Tc}$ . *Nucl Med Commun.* 2001;22:203–215.
  8. Zhang YM, Liu N, Zhu ZH, Rusckowski M, Hnatowich DJ. Influences of different chelators (HYNIC, MAG3 and DTPA) on tumor cell accumulation and mouse biodistribution of technetium-99m labeled to antisense DNA. *Eur J Nucl Med.* 2000;27:1700–1707.
  9. Decristoforo C, Mather SJ. Preparation,  $^{99m}\text{Tc}$  labeling, and in vitro characterization of HYNIC and N3S modified RC-160 and [Tyr<sub>3</sub>]octreotide. *Bioconj Chem.* 1999;10:431–438.
  10. Decristoforo C, Mather SJ. Technetium-99m somatostatin analogues: effect of labeling methods and peptide sequence. *Eur J Nucl Med.* 1999;26:869–876.
  11. Babich JW, Fischman AJ. Effect of “co-ligand” on the biodistribution of  $^{99m}\text{Tc}$ -labeled hydrazinonicotinic acid derivatized chemotactic peptides. *Nucl Med Biol.* 1995;22:25–30.
  12. Roberts BL, Markland W, Ley AC, et al. Directed evolution of a protein: selection of potent neutrophil elastase inhibitors displayed on M13 fusion phage. *Proc Natl Acad Sci USA.* 1992;89:2429–2433.
  13. Hnatowich DJ, Layne WW, Childs RL, et al. Radioactive labeling of antibody: a simple and efficient method. *Science.* 1983;220:613–615.
  14. Abrams MJ, Juweid M, tenKate CI, et al. Technetium-99m-human polyclonal IgG radiolabeled via the hydrazino nicotinamide derivative for imaging focal sites of infection in rats. *J Nucl Med.* 1990;31:2022–2028.
  15. Rusckowski M, Qu T, Pullman J, et al. Inflammation/infection imaging with a  $^{99m}\text{Tc}$ -neutrophil elastase inhibitor in monkeys. *J Nucl Med.* 2000;41:363–374.
  16. Hnatowich DJ, Qu T, Chang F, Ley AC, Ladner RC, Rusckowski M. Labeling peptides with technetium-99m using a bifunctional chelator of a N-hydroxysuccinimide ester of mercaptoacetyltryglycine. *J Nucl Med.* 1998;39:56–64.
  17. Hnatowich DJ, Virzi F, Fogarasi M, Winnard P Jr, Rusckowski M. Can a cysteine challenge assay predict the in vivo behavior of  $^{99m}\text{Tc}$ -labeled to antibodies? *Nucl Med Biol.* 1994;21:1035–1044.
  18. Mardirossian G, Wu C, Rusckowski M, Hnatowich DJ. The stability of technetium-99m directly labeled to an Fab' antibody via stannous ion and mercaptoethanol reduction. *Nucl Med Commun.* 1992;13:503–512.
  19. Fritzberg AR, Kasina S, Eshima D, Johnson DL. Synthesis and biological evaluation of technetium-99m-MAG3 as a hippuran replacement. *J Nucl Med.* 1986;27:111–116.

